

ARTICLE | DOI: 10.5584/jiomics.v14i3.234

## Computational Screening of Natural Compounds as Antiviral Candidates Targeting the SARS-CoV-2 Main Protease

Ilyes Zatla<sup>1,\*</sup>, Lamia Boublenza<sup>1</sup>

<sup>1</sup>Laboratory of Microbiology applied to the Food industry, Biomedical and the Environment, Faculty of Natural and Life Sciences, Earth and Universe Sciences. Department of Biology. University of Tlemcen, Algeria.

**Available Online:** 31 October 2024

### ABSTRACT

The onset of the global pandemic caused by Severe Acute Respiratory Syndrome Coronavirus 2 (SARS-CoV-2) in Wuhan in December 2019 has led to an urgent need for effective preventive and therapeutic solutions. Among the various approaches explored, natural products have shown potential in the fight against COVID-19. This study employed computational techniques to screen and evaluate six natural antiviral compounds for their effectiveness against the SARS-CoV-2 Main Protease ( $M^{Pro}$ ). By using molecular docking simulations, the interactions between these natural compounds and the target proteins were predicted and analyzed, focusing on factors such as binding affinity, interaction patterns, and structural compatibility within the active sites. The analysis indicated that Cladosin C and Rhodatin formed the most stable interactions with  $M^{Pro}$ , engaging with several critical residues. Cannabidiol, Capsaicin, and Kappa-Carrageenan also demonstrated promising interactions, though with some variability. On the other hand, Astaxanthin exhibited the least stable binding, suggesting limited antiviral potential. This research provides insights into the possible roles of these natural compounds as antagonists of the SARS-CoV-2  $M^{Pro}$  enzyme. Further *in vitro* and *in vivo* studies are necessary to confirm the antiviral properties of these compounds, and future research should investigate their broader antiviral applications.

**Keywords:** SARS-CoV-2, COVID-19, Main protease, Biomolecules, Molecular dynamics.

### Introduction

The Severe Acute Respiratory Syndrome Coronavirus 2 (SARS-CoV-2), virus's ability to infect both humans and various mammalian species by exploiting different angiotensin-converting enzyme 2 (ACE2) membrane proteins has underscored its significant impact [1-3]. In response, substantial resources have been dedicated to developing vaccines and therapeutic treatments. This has resulted in the rapid development of several effective vaccines and the advancement of numerous potential treatments through clinical trials. These therapies primarily target viral proteins, including key viral enzymes, or host proteins crucial for viral entry, reflecting a dual approach to combating the virus [4].

Promising strategies including natural products have been involved in the fight against COVID-19 due to their diverse bioactive compounds derived from medicinal plants, animals, and marine sources. This study employs computational

methods to screen and evaluate natural antiviral compounds for their effectiveness against the SARS-CoV-2 Main Protease ( $M^{Pro}$ ) [5, 6]. By performing molecular docking simulations, the study aims to predict and analyze the interactions between these compounds and the viral target proteins. Additionally, an ADEMETS (absorption, distribution, metabolism, excretion, toxicity) report will be used to assess the viability of these compounds. The findings from this research are expected to offer valuable insights and potential leads for future experimental validation and drug design efforts, contributing to the ongoing battle against COVID-19.

### Materials and methods

In this study, we conducted an analytical *in silico* study to investigate the binding interactions between six natural molecules derived from different natural organisms against the target protein of the SARS-CoV-2 virus. The study employed computational docking techniques to predict and

\*Corresponding author: Ilyes Zatl, ilyes.zatla@univ-tlemcen.dz, Tel: +213-5403-15422

analyze the binding modes and affinities of the ligands within the target protein active sites, aiming to identify potential ligand-receptor interactions and gain insights into the binding mechanisms.

ADMET characteristics (absorption, distribution, metabolism, excretion, Toxicity) profiling validation, were utilized using the pkCSM package to identify molecules with favorable properties for oral bioavailability and potential as medications within the body, to predict the toxic effects of compounds, while also assessing their drug-like physical and chemical properties.

**Preparation of Ligand Structures:** Six natural molecules were chosen according to their antiviral characteristics from the literature, where we included two plant molecules [7, 8], Cannabidiol (from *Cannabis sativa*) and Capsaicin (from *Capsicum annuum*), two fungi molecules [9], Cladosin C (from microfungi *Cladosporium sphaerospermum*) and Rhodatin (from macrofungi *Rhodotus palmatus*), also, two algae molecules [10], Astaxanthin (from green microalgae *Haematococcus pluvialis*) and Kappa-Carrageenan (from red marine macroalgae *Kappaphycus alvarezii*) were selected as ligands. The structures of these six molecules were retrieved from the PubChem database, and further processed and optimized using ChemDraw and Chimera software.

ChemDraw was employed for drawing and editing the initial ligand structures, which facilitated the accurate representation of the ligands based on the available information from PubChem.

UCSF Chimera [11] was utilized to optimize the ligand structures, including energy minimization and geometry optimization, leading to more reliable and physiochemically reasonable conformations.

**Preparation of Receptor Structures:** The structure of the Main protease was retrieved from the PDB database and saved as PDB files.

The catalytic domains were selected for inhibitor docking of inhibitors against the SARS-CoV-2 targets using PyMol (The PyMOL Molecular Graphics System, Version 1.2r3pre, Schrödinger, LLC), as well as according to literature [12].

The 3C-like protease ( $M^{pro}$ ) catalytic sites: THR190, HIS41, CYS145, GLU166, GLY143, PHE140.

**Grid Generation:** To define the binding sites for docking, grids were generated around the active sites of the SARS-CoV-2 proteins, namely the Main Protease. The grid parameters, including size, spacing, and center coordinates, were set using the AutoGrid module of AutoDock [13].

**Docking Protocol:** All the retrieved compounds were docked using the selected catalytic site of the three-dimensional structure. The ligands were prepared by adding polar hydrogens, merging nonpolar hydrogens, and assigning partial charges using AutoDock Tools [14]. The

prepared ligands were then docked into the binding sites of the SARS-CoV-2 proteins using AutoDock Vina [15]. Multiple docking runs were conducted to explore different ligand conformations and orientations within the binding sites.

**Post-Docking Analysis:** After the docking simulations, the resulting poses were analyzed to identify potential ligand-receptor interactions and select the most favorable binding conformations. The docking results were visually inspected and analyzed using molecular visualization software AutoDock Tools. The binding poses were assessed based on their binding energies, ligand-receptor interactions, and conformational fit within the active site.

**Molecular dynamics simulations:** Schrödinger LLC Desmond software [16, 17] was employed for performing molecular dynamics (MD) simulations for a duration of 100 nanoseconds [18]. Prior to the MD simulation, a crucial step involved the protein-ligand docking, which predicted the static binding position of the ligand molecule at the active site of the protein as mentioned before [19]. MD simulations, incorporating Newton's classical equation of motion, simulate the movement of atoms over time and provide insights into the dynamic behavior and ligand-binding status in a physiological environment [20].

The ligand-receptor complex was preprocessed using Maestro's Protein Preparation Wizard, which performed optimization, minimization, and filling of any missing residues as necessary. The system was constructed using the System Builder tool. The MD simulation employed the TIP3P (Intermolecular Interaction Potential 3 Points Transferable) solvent model, utilizing an orthorhombic box with a temperature of 300 K, pressure of 1 atm, and the OPLS\_2005 force field [21]. To maintain physiological conditions, counter ions were introduced, and the system was neutralized using 0.15 M sodium chloride. Before the simulation, the models were equilibrated, and trajectories were recorded at regular intervals of 100 ps for subsequent analysis and inspection.

## Results and Discussion

Six natural products; Astaxanthin, Cannabidiol, Capsaicin, Cladosin C, Rhodatin, and Kappa-Carrageenan were tested against SARS-CoV-2 target  $M^{pro}$  (PDB ID. 7CAM). To test the relative stability of the 6 ligands, a 100 ns MD simulation was performed for the six complexes using Desmond in the Schrödinger package [16, 17].

**ADMET characteristics:** The ADMET properties of the selected six molecules are represented in Table 1. These properties fulfil the Lipinski's rule criteria and the extra condition on the number of rotatable bonds, suggesting their good pharmacokinetic permeability and their oral bioavailability [22, 23].

**Table 1** - ADMET characteristics of the six biomolecules predicted by pkSCM package.

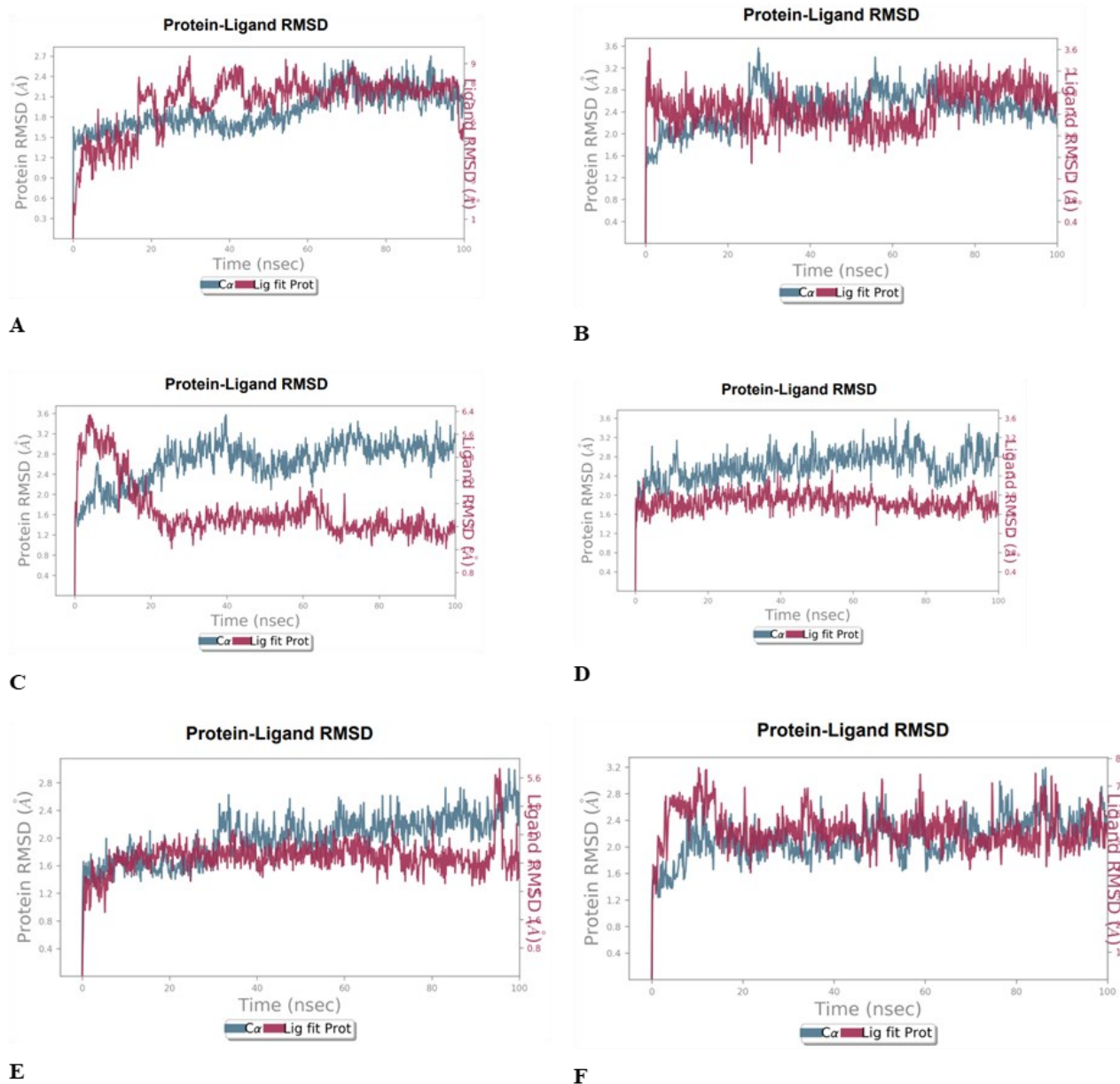
Kappa-Carrageenan	Rhodatin	Cladosin C	Capsaicin	Cannabidiol	Astaxanthin	Molecule
368.368	398.455	250.298	305.418	314.469	598.868	MOL_WEIGHT
3.06828	3.4701	1.56907	3.7896	5.8465	9.1294	LOGP
5	1	4	9	6	11	ROTATABLE_BONDS
5	6	4	3	2	4	ACCEPTORS
3	3	4	2	2	2	DONORS
154.397	169.004	106.029	132.74	140.109	265.976	SURFACE_AREA
-3.011	-3.635	-2.147	-3.842	-3.396	-6.127	Watersolubility
524	562	-256	1.338	956	827	Caco2 permeability
81.971	91.746	72.937	92.836	91.534	93.641	Intestinal absorption (human)
-2.894	-2.827	-2.755	-3.133	-2.764	-2.659	Skin Permeability
Yes	Yes	No	Yes	Yes	Yes	P-glycoprotein substrate
No	Yes	No	No	Yes	No	P-glycoprotein I inhibitor
No	Yes	No	No	No	Yes	P-glycoprotein II inhibitor
0.59	42	-0.37	142	618	-784	VDs (human)
248	0.04	474	115	0.04	0	Fraction unbound (human)
-1.025	-802	-939	-411	7	395	BBB permeability
-2.962	-2.327	-3.421	-2.328	-1.293	-1.383	CNS permeability
No	No	No	No	No	No	CYP2D6 substrate
No	Yes	No	Yes	No	Yes	CYP3A4 substrate
No	No	No	Yes	Yes	No	CYP1A2 inhibitor
No	No	No	No	No	No	CYP2C19 inhibitor
No	No	No	Yes	No	No	CYP2C9 inhibitor
No	No	No	No	No	No	CYP2D6 inhibitor
No	No	No	Yes	No	No	CYP3A4 inhibitor
218	319	332	1.294	1.165	849	Total Clearance
No	No	No	No	No	No	Renal OCT2 substrate
No	No	No	No	No	No	AMES toxicity
-317	-759	257	302	-202	-424	Max. tolerated dose (human)
No	No	No	No	No	No	hERG I inhibitor
No	No	No	Yes	Yes	No	hERG II inhibitor
1.953	2.61	2.726	2.566	2.35	4.061	Oral Rat Acute Toxicity (LD50)
1.472	1.909	1.31	1.85	2.517	2.28	Oral Rat Chronic Toxicity (LOAEL)
Yes	No	No	No	No	No	Hepatotoxicity
No	No	No	No	No	No	Skin Sensitisation
392	289	61	1.511	893	313	T. Pyriformis toxicity

Figure 1 gives insight towards the binding stability of the 6 target ligands against SARS-CoV-2 M<sup>PRO</sup> using Root Mean Square deviation (RMSD) plots for both protein backbone and the ligand. Protein C $\alpha$  RMSD represents the stability of the protein when the ligand binds to it. The less fluctuation the more stability it possesses. Similarly, ligand RMSD represents the ligand stability upon binding to the target protein. As shown in figure 1, all the 6 ligands showed very good binding stability with low oscillations where cladosin C and rhodatin seems to have the best RMSD with fluctuation around 1.6 Ao (figure 1.D and E). Also, capsaicin (figure 1.C) showed a stable binding conformation after 20 ns from the

beginning of the simulation where in the last 80 ns RMSD of both the protein backbone and capsaicin were oscillating between 1 and 1.4 Ao which is a good indication for their stable binding. Both cannabidiol and Kappa-carrageenan (figure 1.B and 1.F, respectively) possess a higher but still acceptable RMSD fluctuation range; between 1.6 and 3.2 Ao, for both complexes. On the other hand, astaxanthin bound to M<sup>PRO</sup> was found to be the least stable complex where in the first 20 ns upon astaxanthin binding to M<sup>PRO</sup> shows a high fluctuation between 0.9 and 1.8 Ao and the second 40 ns show also a relatively non-stable binding with a reported RMSD ranging between 1.3 and 2.7 Ao while only in the last

40 ns this binding starts to be relatively stable; oscillating through plotting the Root Mean Square fluctuation (RMSF) of each complex where green-colored vertical bars represent the residues involved in the interaction. Secondly, the ligand-protein interactions with each residue are categorized into four types of interactions: Hydrogen bonds, hydrophobic interactions, ionic interactions and water bridges. Also, the

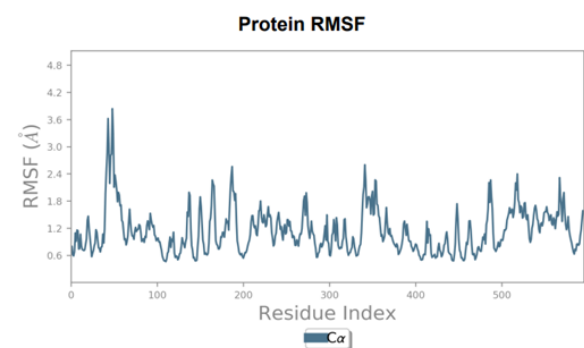
A deeper insight for the contact of each ligand towards M<sup>Pro</sup> target was evaluated via studying the protein amino acids involved in binding interactions formed with each ligand



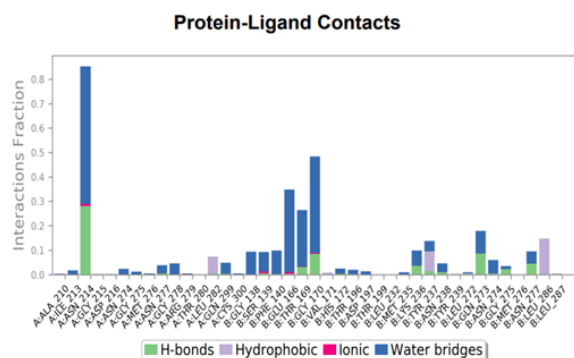
**Figure 1** - The structural dynamics of six ligands—astaxanthin (A), cannabidiol (B), capsaicin (C), cladosin C (D), rhodatin (E), and Kappa-carrageenan (F)—were examined in relation to their binding with SARS-CoV-2 Main Protease (M<sup>Pro</sup>) (PDB ID: 7CAM). The analysis included calculating the backbone C $\alpha$  Root Mean Square Deviation (RMSD) (depicted in blue) and the ligand RMSD (shown in red) throughout a 100-nanosecond molecular dynamics simulation.

total number of contacts formed between the ligand and its target protein was plotted throughout the 100 ns trajectories and a schematic diagram for ligand 2D atomic interactions with each protein residue in each trajectory frame (0 through 100 ns) was presented for each complex. RMSF of  $M^{Pro}$  in complex with astaxanthin show high fluctuation with no reported interaction (no green bars) throughout the whole 100 ns meaning that no stable binding (figure 2.A) and this is confirmed through 2D ligand-protein contact shown in figure 2.E that also shows no interaction with the pocket residues. Figure 2.B shows the interaction fraction the ligand can form with the pockets' residues. It is noticeable that only Asn 214

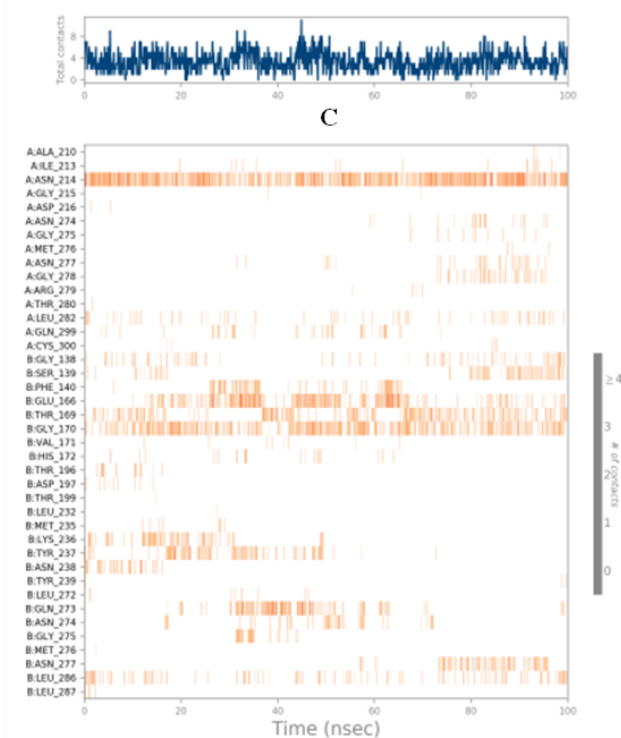
was able to form a good contact with astaxanthin being able to form H-bond interaction with a fraction of about 0.3 and this was confirmed in figure 2.D where only Asn 214 was able to maintain a good interaction with astaxanthin throughout the whole simulation. Thr 169 and Gly 170 also were able to form H-bonds with astaxanthin but they were observed to be very weak (with interaction fraction less than 0.1) figure 2.B and also cannot be maintained during the simulation figure 2.D. Accordingly, no significant interaction is reported for astaxanthin- $M^{Pro}$  complex which complies with the complex RMSD plot (figure 1.A).



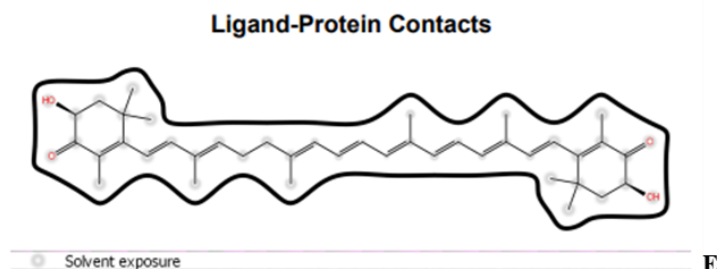
A



B



D



E

**Figure 2** - Structural Dynamics of Astaxanthin with SARS-CoV-2 M<sup>Pro</sup>: (A) Protein RMSF, (B) Interaction Fractions Shown in a Stacked Bar Chart, (C) Timeline of Specific Interactions, (D) Residue-Ligand Interactions per Trajectory Frame, (E) 2D Ligand-Protein Interaction Map.

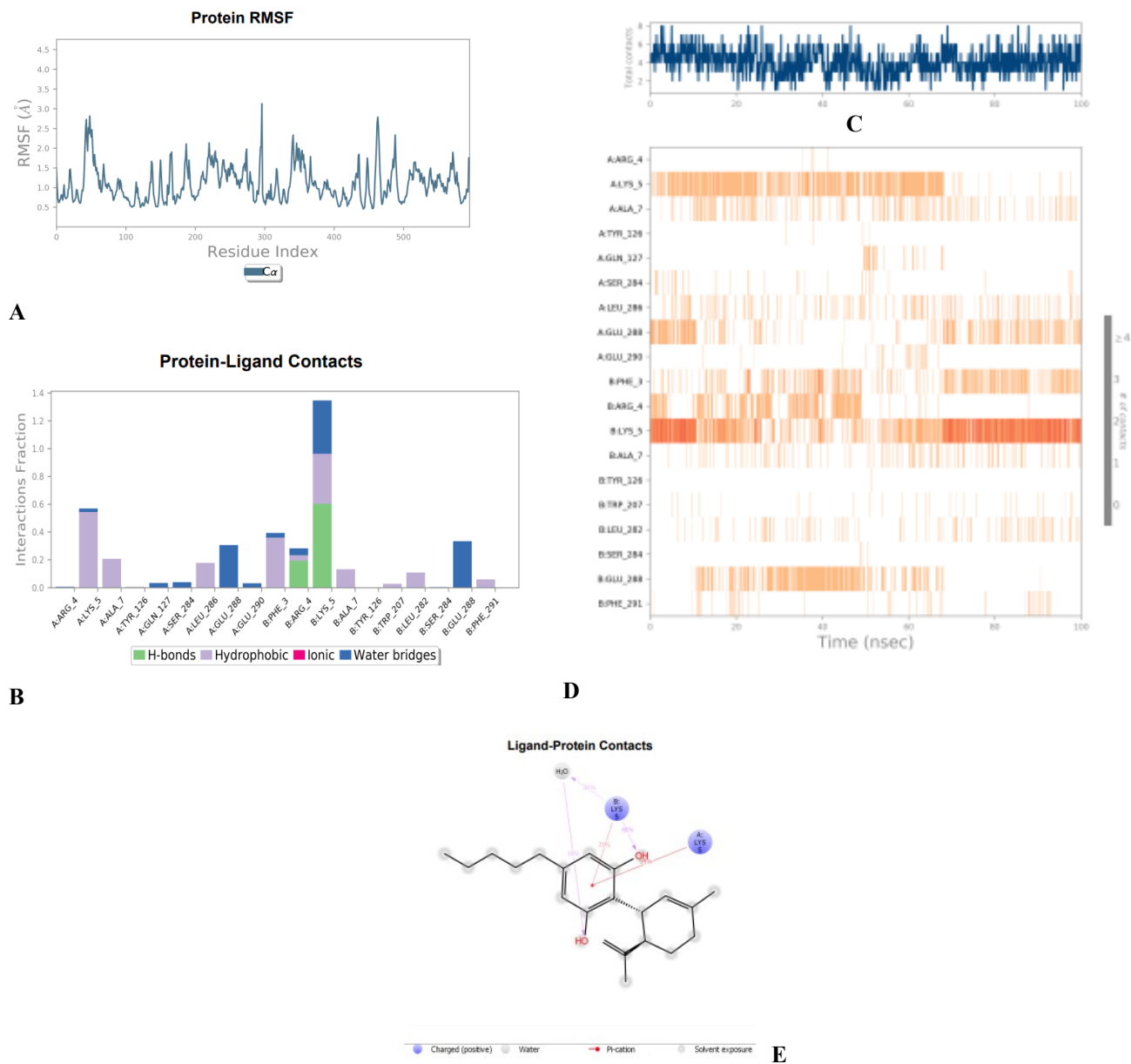
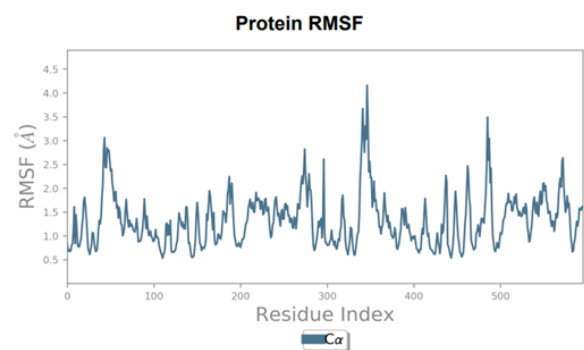


**Figure 3** - Structural Dynamics of Cannabidiol Bound to SARS-CoV-2 M<sup>Pro</sup>: (A) Protein RMSF, (B) Stacked Bar Chart of Protein-Ligand Interaction Fractions, (C) Timeline of Total Specific Interactions, (D) Residue-Ligand Interactions per Trajectory Frame, (E) 2D Map of Ligand-Protein Interactions.

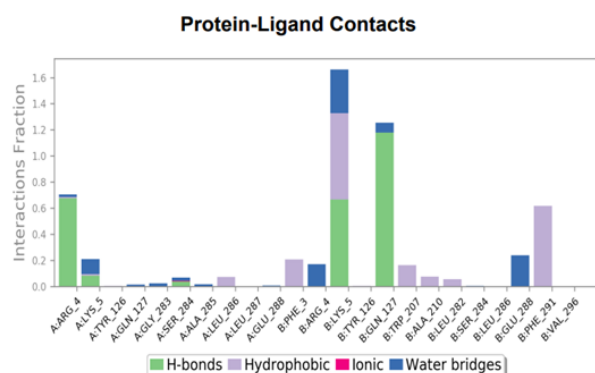
Regarding, cannabidiol-SARS-CoV-2 M<sup>PRO</sup> complex also high protein RMSF was observed indicating unreasonable binding (figure 3.A). Only 2 residues were able to form H-bonds; Arg 4 (interaction fraction = 0.2) and Lys 5 (interaction fraction = 0.6) in chain B also Lys 5 in chain A was a Pi-cation reaction (interaction fraction = 0.55) (figure 3.B). Figure 3.E shows the H-bond formed with Lys 5 in chain B and Pi-cation interaction with Lys 5 in chain A where only interactions that occur more than 30.0% of the simulation are reported. Lys 5 in both chains (a and B) seems to be a key residue responsible for cannabidiol binding against M<sup>PRO</sup> as they are noticed to be formed in most trajectory frames during the 100 ns simulation (figure 3.D).

Similar interactions were observed upon capsaicin binding to M<sup>PRO</sup> (figure 4.E), where also Lys 5 in chain B was able to form

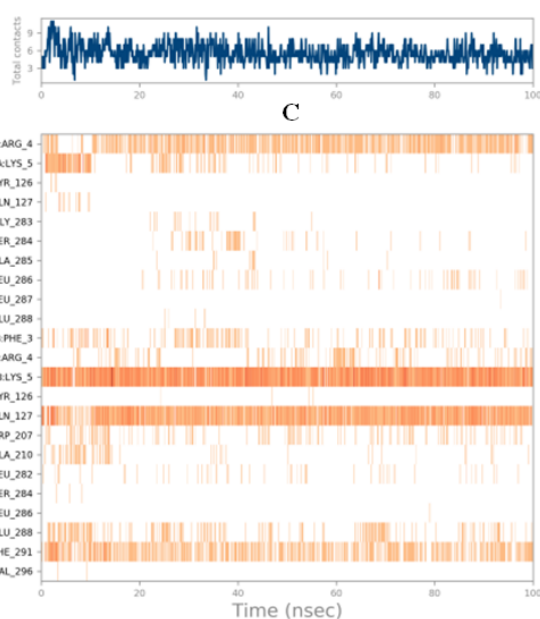
H-bond and Pi-cation interactions with capsaicin showing the highest reported interaction fraction (more than 1.6) (figure 4.B). Also, Lys 5 in chain A was able to form a Pi-cation interaction and was noticed at the first 10 ns from the beginning of the simulation (figure 4.D). Another 2 important residues were reported in this simulation; Arg 4 (chain A) and Gln 127 (chain B) with interaction fractions = 0.7 and 1.3, respectively (fig 4. B). Both were able to form H-bonds with the ligand and these bonds were stable during the simulation (figure 4. D). Although good binding interactions are observed for this complex, the protein RMSF is reported to be highly fluctuating (figure 4.A). An explanation for this high residue RMSD fluctuation can be concluded from the RMSD plot shown in figure 1.C, where the complex starts to stabilize its binding interaction 20 ns after the beginning of the simulation.



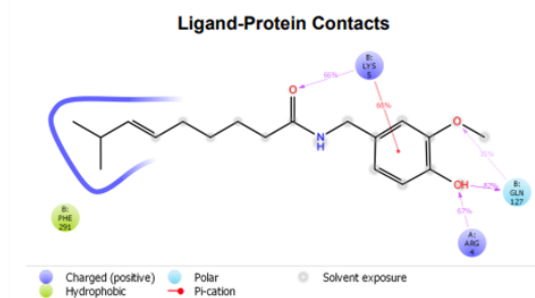
A



B



D



E

**Figure 4** - Structural Dynamics of Capsaicin with SARS-CoV-2 M<sup>PRO</sup>: (A) Protein RMSF, (B) Bar Chart of Protein-Ligand Interaction Fractions, (C) Timeline of Total Specific Interactions, (D) Residue-Ligand Interactions per Trajectory Frame, (E) 2D Ligand-Protein Interaction Map.

As reported previously that cladosin C and rhodatin show the best and the most stable RMSD fluctuation (figure 1.D and E), the best binding interactions were reported for the 2 complexes. Cladosin C and rhodatin were able to form interactions with 6 and 3 residues, respectively, in M<sup>PRO</sup> active pocket. Some of them are previously reported with cannabidiol and capsaicin Lys 5. Also Gln 127 as a key residue was reported when M<sup>PRO</sup> was in complex with capsaicin, cladosin C and rhodatin (figure 5.E and 6.E). A third pocket residue reported with both cladosin C and rhodatin ligands was Leu 282 forming a water bridge with both pockets. Cladosin C was able to form another water bridge with M<sup>PRO</sup> Glu 288 active pocket (figure 5.E). Regarding cladosin C, the highest interaction fraction was observed with Lys 5 (chain B) which was able to form both H-bond and water bridge interactions (figure 5.B). It also possesses the most permanent interaction along the 100 ns simulation (figure 5.D). For rhodatin, Lys 5 (chain A) showed to be the main residue involved in the interaction with interaction fraction of more than 1.75. The second important residue was Gln 127 (interaction fraction > 0.75) (figure 6.B) where both were able to interact with the rhodatin in almost each trajectory frame (figure 6.D). The protein RMSF for both cladosin C and rhodatin complexes with M<sup>PRO</sup> show a low

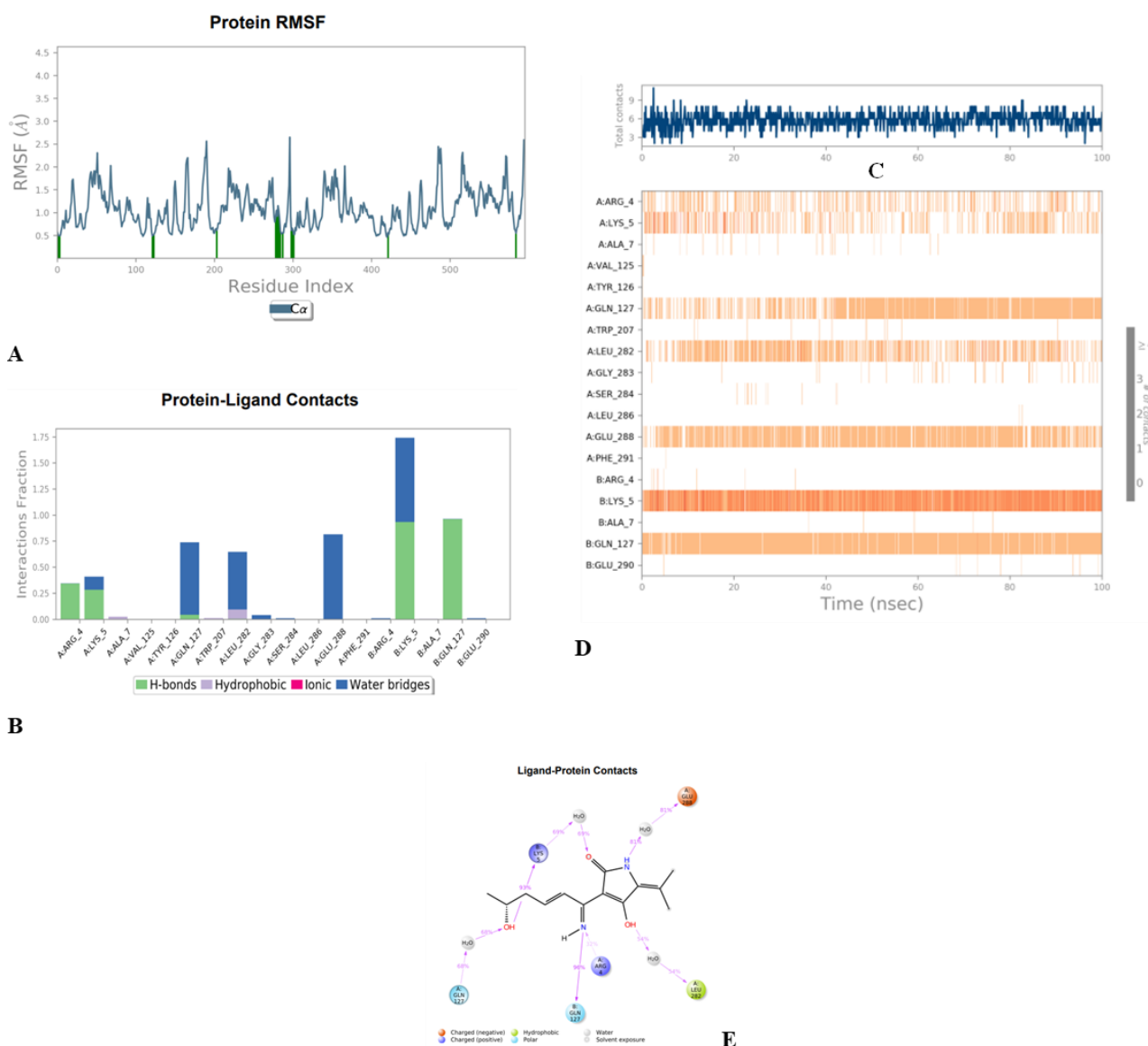


**Figure 5** - Structural Dynamics of Capsaicin with SARS-CoV-2 M<sup>PRO</sup>: (A) Protein RMSF, (B) Bar Chart of Protein-Ligand Interaction Fractions, (C) Timeline of Total Specific Interactions, (D) Residue-Ligand Interactions per Trajectory Frame, (E) 2D Ligand-Protein Interaction Map.

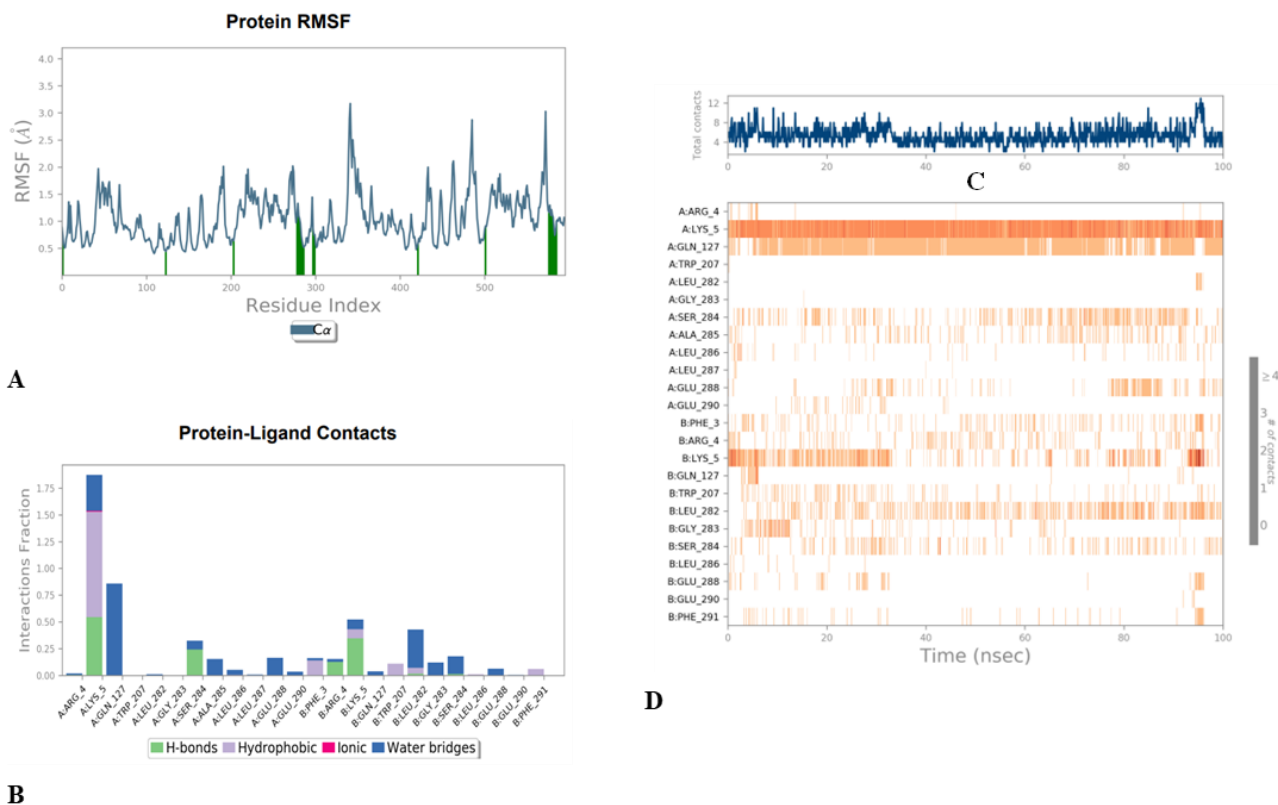
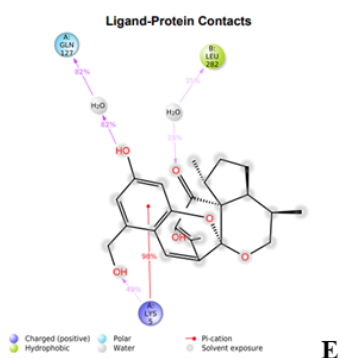


**Figure 6** - Structural Dynamics of Rhodatin with SARS-CoV-2 M<sup>PRO</sup>: (A) Protein RMSF, (B) Stacked Bar Chart of Protein-Ligand Interaction Fractions, (C) Timeline of Specific Interactions, (D) Residue-Ligand Interactions per Trajectory Frame, (E) 2D Ligand-Protein Interaction Map.



fluctuation with the same reported amino acids (shown in green lines in figure 5.A and 6.A).

While Kappa-carrageenan was able to form a stable interaction with M<sup>PRO</sup> pocket residues with a steady stable RMSD (figure 1.F), it shows a different binding mode interacting with different pocket residues. As shown in figure 7.E, 4 residues were involved in this binding interaction; Glu 14, Gly71, Ser 121 and Pro 122. Glu 14 showed the highest interaction fraction (~1.75) followed by both Ser 121 and Pro 122; exhibiting

binding interaction fractions = 1 and 0.75, respectively. These 3 residues were able to interact with the ligand via both H-bond and water bridges (figure 7.B). A fifth important residue which is not reported in 2D interaction is Thr 154. Thr 154 was able to interact Kappa-carrageenan via water bridges and hydrophobic interaction (figure 7.B) and maintained these interactions within most of the trajectory frames (figure 7.D). Also, figure 7.B showed that Ser 121 and Pro 122 maintained their interactions in most of the simulation frames while Glu 14 is almost the main key interaction in through all the 100 ns simulation.

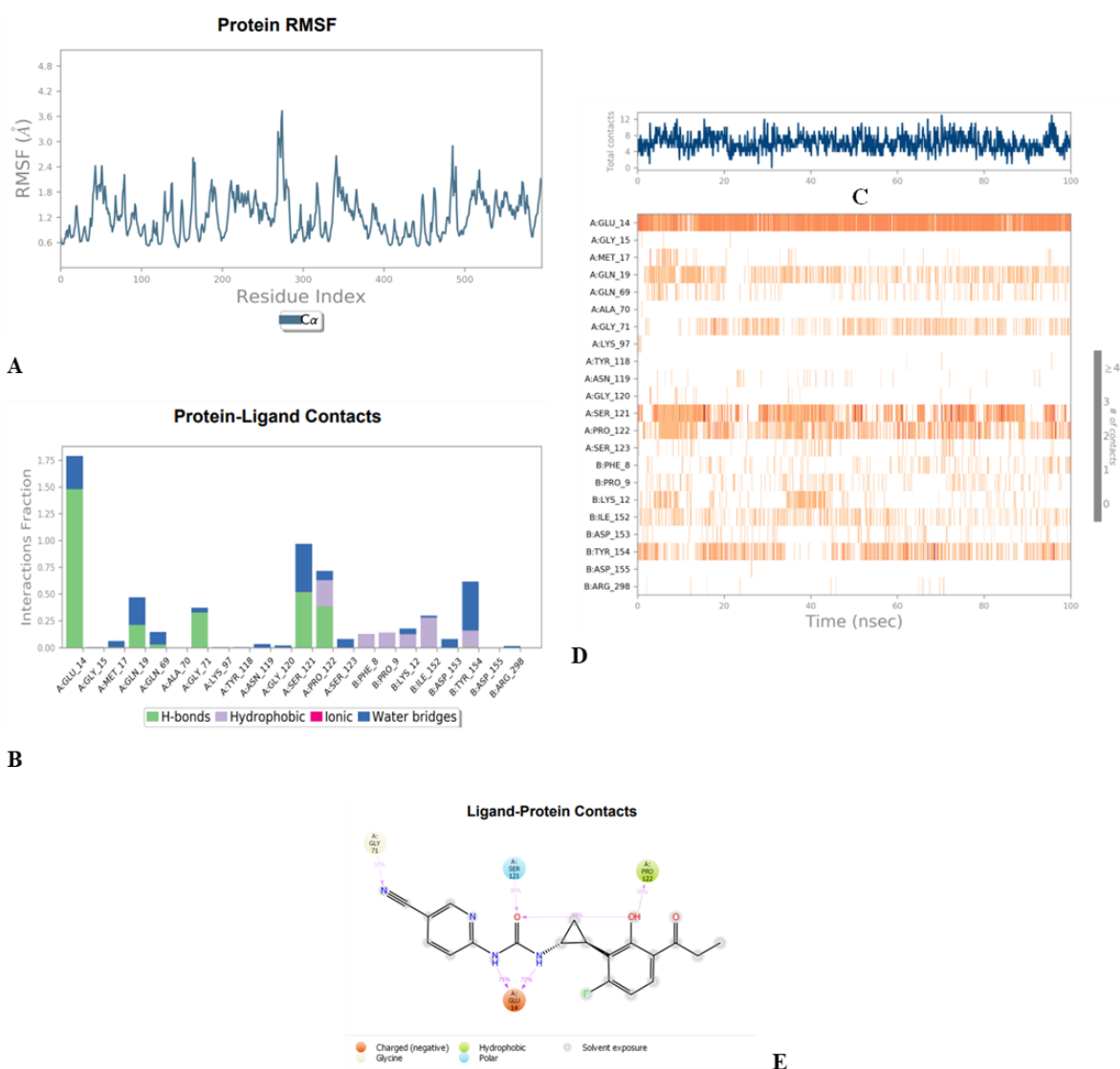


**Figure 7 - Structural Dynamics of Kappa-Carrageenan with SARS-CoV-2 M<sup>PRO</sup>:** (A) Protein RMSF, (B) Stacked Bar Chart of Protein-Ligand Interaction Fractions, (C) Timeline of Specific Interactions, (D) Residue-Ligand Interactions per Trajectory Frame, (E) 2D Ligand-Protein Interaction Map.

## Conclusion

In the quest to combat the devastating impact of SARS-CoV-2, this study undertook a comprehensive investigation of natural antiviral compounds, focusing on their interactions with the critical viral target, the Main Protease (M<sup>Pro</sup>). Six natural molecules, including Astaxanthin, Cannabidiol, Capsaicin, Cladosin C, Rhodatin, and Kappa-Carrageenan, were assessed using a combination of molecular docking simulations and molecular dynamics. This research has shed light on their potential as antagonists against the viral M<sup>Pro</sup> enzyme. Among these compounds, Cladosin C and Rhodatin emerged as the most promising, demonstrating stable binding interactions with M<sup>Pro</sup> and forming crucial associations with key residues. Cannabidiol, Capsaicin, and Kappa-Carrageenan also showed encouraging interactions, though with some variability in stability. On the other hand, Astaxanthin exhibited the least stable binding, suggesting limited potential as an antiviral agent against SARS-CoV-2. These findings contribute to our understanding of the stability and efficacy of these natural compounds as potential antiviral agents. The next step is to validate these computational results through in vitro and in vivo studies, offering a pathway for the development of novel antiviral therapies in the ongoing battle against COVID-19. This research also underscores the importance of further exploration of natural sources containing these compounds, potentially uncovering new sources of antiviral agents.

## Ethics approval and consent to participate

Not applicable.

## Consent for publication

Not applicable.

## Availability of data and materials

The data that support the findings of this study are available from the corresponding author upon request.

## Competing interests

The authors declare no conflict of interest.

## Funding

This research received no external funding.

## Authors contributions

Ilyes Zatl: Conceptualization, Literature search, data collection, data analysis, manuscript writing, manuscript editing. Lamia Boublenza: Manuscript review, supervision of the project.

## Acknowledgments

We would like to Thank Dr. Somdutt Mujwar from Chitkara University of India for proofreading the manuscript.

## References

- [1] Carabelli, A.M., Peacock, T.P., Thorne, L.G. et al. SARS-CoV-2 variant biology: immune escape, transmission and fitness. *Nat Rev Microbiol*, 2023, 21, 162–177.
- [2] Zatl I, Boublenza L, Hassaine H. SARS-CoV-2 origin, classification and transmission: a mini-review. *Curr Top Virol*. 2021; 18: 31-38.
- [3] Zatl I, Boublenza L, Hassaine H. SARS-CoV-2 morphology, genome, life cycle and our bodies' immune response: a review. *Curr Top Virol*. 2021; 18: 15-24
- [4] Li, G., Hilgenfeld, R., Whitley, R. et al. Therapeutic strategies for COVID-19: progress and lessons learned. *Nat Rev Drug Discov*, 2023, 22, 449–475.
- [5] Zatl, I., & Boublenza, L. In Silico Evaluation of Natural Antiviral Compounds Targeting the RBM of SARSCoV-2 Spike Glycoprotein. *Trop J Nat Prod Res*, 2023, 7(10), 4273–4283.
- [6] Wang, Z., Wang, N., Yang, L., Song, X-q. Bioactive natural products in COVID-19 therapy. *Front Pharmacol*, 2022, 13:926507.
- [7] Holst, M., Nowak, D., Hoch, E. Cannabidiol As a Treatment for COVID-19 Symptoms? A Critical Review. *Cannabis Cannabinoid Res*, 2023, 487-494.
- [8] Alrasheid, A.A., Babiker, M.Y., Awad, T.A. Evaluation of certain medicinal plants compounds as new potential inhibitors of novel corona virus (COVID-19) using molecular docking analysis. *In Silico Pharmacol*, 2021, 9, 10.
- [9] Takahashi, J. A., Barbosa, B. V. R., Lima, M. T. N. S., Cardoso, P. G., Contigli, C., Pimenta, L. P. S. Antiviral fungal metabolites and some insights into their contribution to the current COVID-19 pandemic. *Bioorganic & Medicinal Chemistry*, 2021, 46, 116366.
- [10] Carbone, D.A., Pellone, P., Lubritto, C., Ciniglia, C. Evaluation of Microalgae Antiviral Activity and Their Bioactive Compounds. *Antibiotics*, 2021, 10(6), 746.
- [11] Pettersen, E.F., Goddard, T.D., Huang, C.C., Couch, G.S., Greenblatt, D.M., Meng, E.C., Ferrin, T.E. *J Comput Chem*. 2004 (13):1605-12.
- [12] Andola, P., Pagag, J., Laxman, D. et al. Fragment-based inhibitor design for SARS-CoV2 main protease. *Struct Chem*, 2022, 33, 1467–1487.

- [13] Goodsell, D. S. and Olson, A. J. Automated Docking of Substrates to Proteins by Simulated Annealing. *Proteins: Structure Function Genetics*, 1990, 8: 195-202.
- [14] Morris, G. M., Huey, R., Lindstrom, W., Sanner, M. F., Belew, R. K., Goodsell, D. S. and Olson, A. J. Autodock4 and AutoDock-Tools4: automated docking with selective receptor flexibility. *J. Computational Chemistry*, 2009, 16: 2785-91.
- [15] O. Trott, A. J. Olson, AutoDock Vina: improving the speed and accuracy of docking with a new scoring function, efficient optimization and multithreading. *J. Computational Chemistry*, 2010, 31, 455-461
- [16] Schrödinger, E., Schrödinger. Centenary Celebra, 2016.
- [17] Schrödinger, L., DE Shaw Research, New York, Maestro-Desmond Interoperability Tools, Schrödinger New York, NY, USA, 2020.
- [18] Ferreira, L.G., et al., Molecular docking and structure-based drug design strategies. *Molecules*, 2015, 20(7): 13384-421.
- [19] Hildebrand, P.W., A.S. Rose, and J.K.S. Tiemann, Bringing Molecular Dynamics Simulation Data into View. *Trends Biochem Sci*, 2019, 44(11): 902-913.
- [20] Rasheed, M.A., et al., Identification of Lead Compounds against Scm (fms10) in *Enterococcus faecium* Using Computer Aided Drug Designing. *Life (Basel)*, 2021 11(2).
- [21] Shivakumar, D., et al., Prediction of Absolute Solvation Free Energies using Molecular Dynamics Free Energy Perturbation and the OPLS Force Field. *J. Chemical Theory and Computation*, 2010, 6(5): 1509-1519.
- [22] Pollastri, M.P. Overview on the Rule of Five. *Curr ProtOC Pharmacol*, 2010, 49.
- [23] Douglas, E.V., Pires, T.L., Blundell, D.B. Ascher pkCSM: predicting small-molecule pharmacokinetic properties using graph-based signatures. *J. Medicinal Chemistry*, 2015, 58(9), 4066–4072.